accepted for ApJ

Images of the hot spots in Cygnus A at 87 GHz

M.C.H. Wright[1], L.M. Chernin[1,2], and J.R.Forster[1]

ABSTRACT

We used the BIMA array to map Cygnus A at 87 GHz with 0.4″ angular resolution. The hot spots at the working surfaces in the radio lobes show spectral index gradients from -0.6 to -1.1 between 87 and 5 GHz, suggesting significant synchrotron aging within the hot spots. The data do not show a marked spectral break between 5 and 87 GHz however, suggesting a continuous injection of high energy relativistic particles into both compact and extended hotspots on time scales less than 30 Kyr.

Subject headings: galaxies: individual (Cygnus A) — radio continuum: galaxies — techniques: interferometric

1. Introduction

Cygnus A is the closest example of a powerful double radio galaxy. It is identified with a cD galaxy at z=0.057, giving an angular scale of 1″ = 1 kpc (Ho = 75 km/s/Mpc). Cygnus A has been extensively imaged at frequencies from 150 MHz to 100 Ghz with interferometer arrays providing sufficient angular resolution to map the structure of the radio lobes. At high frequencies the maps are dominated by the hot spots at the ends of the radio lobes. The hot spots are thought to be the working surfaces of a jet originating in the nucleus of the central galaxy. Images of the radio lobes from 1.4 to 15 GHz (Carilli 1989) reveal a complex structure, with two kpc-sized hot spots at the head of each 60 kpc radio lobe, and spectral gradients which correspond to synchrotron aging of the high energy electrons in the radio lobes (Carilli etal, 1991). The radiative lifetime of the relativistic electrons in the hot spots (30,000 years at 87 GHz) is much less than the light travel time from the nucleus, requiring acceleration of the electrons within the hot spots, or deposition there via the jet. The relationship between the pairs of hot spots within a lobe is not clear. The currently accepted model is the "dentist drill" model, where the jet changes direction in time scales short compared with the source lifetime (Scheuer, 1982; Williams and Gull, 1985). Comparison of high resolution images at the highest frequency possible with maps at lower frequency reveals where high energy particles are being generated, distinguishing between the various models and providing a fundamental test of synchrotron spectral aging theory. In this letter we present 0.4″ resolution imaging of Cygnus A at 87 GHz obtained with the BIMA array[3] and compare our results with VLA images at 5 and 15 GHz at similar resolution.

---

[1]Radio Astronomy Lab, University of California, Berkeley, CA 94720

[2]Hitachi Micro Systems, 179 Tasman Dr, San Jose, CA 95134

[3]The BIMA array is operated by the Berkeley-Illinois-Maryland Association under funding from the National Science Foundation

2. Observations

The observations were obtained with the 9-antenna BIMA array in 1996 Feb - April (Welch et al., 1996). Cygnus A was observed using three configurations of the antennas providing 108 antenna separations from 6.3 to 1310 m. In order to accurately image the full $2'$ extent of the radio lobes we observed 3 pointings centered close to the nucleus and the hot spots. The observations were made in LCP to avoid sensitivity to linear polarization. The quasar 2007+404 was observed as a phase calibrator at 25 min. intervals for the more compact B and C array configurations. In the extended A configuration 2007+404 was included as an additional pointing center in the mosaic observation in order to provide a phase calibration at 1 minute intervals. We used integration times of 11.5s, 23s and 50s in the A, B and C configurations respectively.

Maps were made with the MIRIAD software package (Wright and Sault, 1993). Initially we used the quasar 2007+404 to calibrate the instrumental phase. The antenna gains were determined from observations of planets at short antenna separations. The 3 pointings were first imaged separately and combined in a linear mosaic. This resulted in images with a dynamic range around 10 (peak to rms). The atmospheric coherence was poor in the A configuration but we were able to improve the dynamic range to 100 by using self-calibration on the unresolved nucleus to calibrate the other two fields.

Each sideband of the local oscillator was used to image the data in an 800 MHz bandwidth. Uniform weighting of the data produced a synthesised beam $0.6 \times 0.4''$ and an rms noise level of 7 mJy, twice the thermal noise level. These images were consistent within the rms noise, so we then combined both sidebands and the 3 pointings in a mosaiced image with a joint deconvolution using a maximum entropy algorithm (Wright and Sault, 1993; Cornwell, 1989).

The dynamic range of the images is limited by pointing errors rather than by thermal noise, or atmospheric phase noise. The primary beam of the 6.1m diameter antennas is approximately Gaussian with a FWHM $132''$ at 87 GHz. A pointing error $d\theta$ results in an amplitude error in the uv-data of $da/a = \theta d\theta/(0.6FWHM)^2$, where a is the amplitude of a source at radius θ in the primary beam. Since the hot spots and nucleus in Cygnus A are each separated by about $60''$, observations centered on each result in one or another of the bright components being close to the half power point in the primary beam. An rms pointing of about $5''$ in both azimuth and elevation axes produceds amplitude errors of about 8% . The effect on the dynamic range in the image depends on the time scale of the pointing errors. The noise level varies approximately as the amplitude error divided by the square root of the number of independent pointing errors. The observed noise level of around 1% is consistent with the observed pointing time scale of about 1 hour.

3. Results

At $0.4''$ resolution, the 87 GHz images of the hot spots are very similar to VLA images at 5 and 15 GHz (Carilli, 1989). In order to compare our results with VLA images to compute spectral index distributions, we rotated the uv-data to B1950 coordinates. Figures 1 and 2 show contours of the 87 GHz emission from the radio lobes. The central source is unresolved with a flux density 0.9 +/- 0.2 Jy. The flux density of the nucleus at 87 GHz is consistent, within the errors, with previous interferometric measurements; there is no evidence for variability at 87 GHz (Wright and Birkinshaw, 1984; Wright and Sault, 1993). The 87 and 5 Ghz images were used to compute the spectral index α, where $S = \nu^{\alpha}$. The spectral index distribution across the hot spots is shown in Figures 3 and 4 superposed on contours of the 5 GHz emission. The spectral index is computed only where both 5 and 87 GHz intensities are greater than 10% of their maximum. A spectral index gradient is clearly seen across all components, with the flattest index -0.6 in the compact hot spots B and E.

A number of systematic errors may affect the derived spectral index distributions: i) incomplete images from poor uv-coverage, ii) flux density scale errors, iii) misalignment of the images. The BIMA and VLA images are very well sampled for structures on the scale of the hot spots. The flux density scale is tied to planet observations. Flux density measurements at different observatories are typically consistent at the 10% level, with a worst error of 20%. The two sidebands which are separated in frequency by 3 Ghz, were independently calibrated; these images were consistent within 10%. The observed spectral gradients are not consistent with errors in the flux density scale. The alignment of the images was compared in two ways; we compared the images from each pointing at 87 GHz, and a mosaic of all 3 pointings interpolated onto a template using the 5 Ghz image. Both methods gave consistent results, with position uncertainties estimated to be about $0.05''$. Note that the separation of the contours is about $0.1''$, so that a misalignment of $0.1''$ corresponds to a 10% flux density error at the peaks of the hot spots, but up to a factor of 2 at the 10% contour on the steep gradients. The corresponding errors in the spectral index between 87 and 5 GHz are $\pm$ 0.05 and $\pm$ 0.35 at the peaks and 10% contours of the hot spots respectively, assuming a constant 10% error at 5 GHz. Clearly the spectral index on the steep edges of the hot spots is to be treated with caution. Finally note that the observed gradients are not consistent with a simple rotation or shift of the images. We conclude that they are real.

4. Discussion

The hot spots are clearly resolved at 87 GHz. The compact components B and E are extended along the jet axis; the more extended components A and D are resolved into a number of ridges transverse to the jet axis. The same structures are seen at 5, 15, and 87 GHz. A Gaussian fitting procedure to the hot spots at $0.4''$ resolution gives almost identical components at 5, 15 and 87 GHz, with positions and FHWM which agree within $0.1''$. The fitted FHWM are $0.6''$ to $2.2''$. In the larger components A and D, the ridges are themselves resolved into double structures orthogonal to the jet axis. The spectral index images (Figures 3 and 4) show a range from -0.6 to -1.1, with the flattest index in the compact hot spots B and E, and steeper in the tail of B. In the extended hot spots A and D the flattest spectral index is found close to the bright ridges, and steepens in a direction towards the nucleus on a scale of 1 kpc. Since the radiative lifetime of the relativistic electrons in the hot spots is around 30,000 years at 87 GHz (Wright and Birkinshaw, 1984), this implies an outflow velocity from the injection site of $\sim$ 0.1 c.

The data are consistent with no spectral break between 5 and 87 GHz at the peaks of all four hot spots. The flat spectrum (α = -0.6) and lack of a spectral break imply a continued injection of relativistic electrons at the peaks on time scales less than 30,000 years. Using the three spectral points at 5, 15 and 87 GHz we do not find a clear spectral break at any point along the direction of the gradients. The data thus suggest high energy particle input throughout the region mapped, rather than injection at discrete points. Detailed modeling using high resolution data at multiple frequencies is required to see if the injection spectra vary across the hotspots.

4.1. Comparison with models

The multiple hotspots in each radio lobe can be explained in the "dentist drill" model (Scheuer, 1982), in which the jet changes direction on time scales short compared with the source lifetime, enlarging the radio lobe. In the "splatter spot" model (Williams and Gull, 1985), the jet first impacts on the lobe cavity walls at primary hot spots B and E, and is deflected to form secondary hot spots A and D. Arguments in favor of the splatter spot model are that multiple hot spots usually occur in pairs with the more compact hot spot recessed from the end of the radio lobe, and with connecting structures and magnetic field directions (Laing, 1989; Carilli, Dreher and Perley, 1989). Our data for Cygnus show that the flattest spectral index is indeed in the compact hot spots B and E, although the spectra are almost as flat in the bright ridges of hot spots A and D. The flat spectra imply that high energy particles are accelerated in the secondary hot spots, or transported there in a highly relativistic jet.

The structure of the secondary hot spots is remarkably similar to the expected double-shock from a supersonic jet ramming into the ambient medium (e.g. Smith etal, 1989). This suggests that the secondary hot spots are also at the working surface of a jet. Most of the emission at 87 GHz comes from the secondary hot spots; evidently the jet deposits most of its energy there. Thus, one problem with the splatter spot model is producing a well collimated outflow from the primary in order to sustain the jet terminus at the secondary. Lonsdale and Barthel (1986) proposed that the jet is re-collimated in a dense, 10^8 M0 intergalactic cloud at the primary and directed towards the secondary. For cygnus A the curved tail of hot spot B may represent the trajectory of the jet towards the secondary, but the pressure gradients are in the wrong sense to produce the curvature. Wilson (1989) points out that supersonic gas jets in the laboratory do not "bounce" off of solid objects, but rather form wall jets. By analogy, an astrophysical jet is more likely to flow along the wall of the lobe cavity until it forms a terminal shock at the end of the lobe forming the secondary hot spot. The hot spots are also a reservoir of energy (Eales, Alexander and Duncan, 1989), suggesting energy input over the lifetime of the source.

The equipartition magnetic fields range from 250 to 350 μG. Similar estimates are obtained from inverse Compton X-ray emission from the hot spots (Harris, Carilli, and Perley 1994). Estimates of the energy density are $\sim 10^{-9}$ ergs cm^{-3} in the hot spots, and $\sim 10^{-10}$ ergs cm^{-3} in the heads of the radio lobes (Carilli and Barthel, 1996). The pressure in the cluster gas is $\sim 10^{-10}$ ergs cm^{-3}, so the hot spots are probably confined by ram pressure. Equating the pressure in the hot spots to the ram pressure of the external X-ray emitting gas with a cluster density 10^{-2} cm^{-3}, we derive an advance rate of 3000 km s^{-1}. The primary hot spot B appears to extend between $1 - 4''$ beyond the lobe envelope suggesting that the jet has persisted in this direction for at least $\sim 3\ 10^5$ years.

The flat spectral index of the ridges in the extended hot spots A and D, requires that they continue to generate high energy particles which radiate at 87 GHz. The similarity in spectra suggests that both compact and extended hot spots are at the working surface of a jet, and confined by ram pressure. Since the jet is hard to trace as it enters the bright heads of the radio lobes, it is possible that the jet is disrupted by backflow from the hot spots and feeds both primary and secondary hot spots. Alternatively, the jet direction may change intermittently on time scales less than 30,000 years; 3-D simulations of a precessing jet lead to structures which contain primary and secondary hot spots which continue to be energized by jet material after a new primary has formed (Cox, Gull and Scheuer, 1991).

5. Summary

1) The images of the hot spots in Cygnus A show the same structures at 5, 15 and 87 GHz at 0.4$''$ resolution.

2) There are spectral gradients across the hot spots, with the flattest spectral index α = -0.6 +/- 0.1 at the peaks of the compact hot spots B and E, and in the bright ridges of hot spots A and D. The spectra steepen in the direction of the nucleus on scales of 1 kpc, implying an outflow velocity away from the injection site of 0.1 c.

3) The spectra derived from images at 5, 15 and 87 GHz are consistent with no spectral break between 5 and 87 GHz at the peaks of the hot spots, and favor continuous injection of relativistic electrons into all the hot spots on time scales of 30,000 years.

4) The agreement in the structure of hot spots A and D with double-shock models favors models in which A and D are powered directly by a jet rather than "secondary splatter spots" powered by an outflow from "primary" hot spots B and E.

This work was supported in part by NSF Grant AST 93-20238 to the University of California. We thank C. Carilli for providing VLA Cygnus A images in digital format.

REFERENCES

Carilli,C.L., Perley,R.A., Dreher,J.W., & Leahy,J.P., 1991, ApJ, 383, 554

Carilli,C.L., & Barthel, P.D., 1996, A&A Rev. 7, 1

Carilli, C.L. 1989, Ph.D. Thesis, Massachusetts Institute of Technology.

Carilli, C.L., Dreher, J.W., & Perley, R.A., 1989, in Hot Spots in Extragalactic Radio Sources, eds. K.Meisenheimer and H.J.Roser (Heidelberg: Springer), p. 51

Cornwell, T.J., 1989, Synthesis Imaging in Radio Astronomy. Ed. R.A. Perley, F.R. Schwab, & A.H.Bridle, ASP Conf. Ser. 6, 277

Cox, C,I., Gull, S.F., & Scheuer, P.A.G., 1991, MNRAS, 252, 558

Eales, S.A., Alexander, P., & Duncan, W.D., 1989, MNRAS, 240, 817

Harris, D.E., Carilli, C.L., Perley, R.A. 1994, *Nature* 367, 713

Harris, D.E., & Carilli, C.L., 1996, in *Cygnus A: Study of a Radio Galaxy*, eds. C.L. Carilli and D.E. Harris (Cambridge: CUP) p. 136

Laing, R.A., 1989, in Hot Spots in Extragalactic Radio Sources, eds. K.Meisenheimer and H.J.Roser (Heidelberg: Springer), p. 27

Lonsdale, C.J., & Barthel, P.D., 1986, AJ 92, 12

Scheuer, P.A.G., 1982, in Extragalactic Radio Sources, IAU Symposium 97, eds. D.Heeschen and C.Wade (Dordrecht: Reidel) p. 163

Smith, M.D., Norman, M.L., Winkler, K-H. A., and Smarr, L., 1985, MNRAS 214, 67

Welch, W.J., Thornton,D.D., Plambeck,R.L., Wright,M.C.H., etal., 1996, PASP, 108, 93

Williams, A.G., & Gull, S.F., 1985, Nature, 313, 34

Wilson, M.J., 1989, in Hot Spots in Extragalactic Radio Sources, eds. K.Meisenheimer and H.J.Roser (Heidelberg: Springer), p. 215

Wright, M.C.H. & Birkinshaw, M. 1984, ApJ, 281, 135

Wright, M.C.H. & Sault, R.J., 1993, ApJ, 402, 546

This preprint was prepared with the AAS LaTeX macros v4.0.

Fig. 1.— North West hot spots A and B. Contour interval 20 mJy, with additional contours at 10 mJy. The beam FWHM is indicated in the lower right corner.

Fig. 2.— South East hot spots D and E. Contour interval 25 mJy.

Fig. 3.— North West hot spots A and B. Spectral index between 5 and 87 GHz gray scale superposed on contours of 5 GHz emission. Contour interval 0.5 Jy, with additional contours at 0.1 and 0.2 Jy.

Fig. 4.— East hot spots D and E. Spectral index 5 and 87 GHz gray scale superposed on contours of 5 GHz emission. Contour interval 0.5 Jy, with additional contours at 0.1 and 0.2 Jy.

Fig. 5.— fig1 - North West hot spots A and B

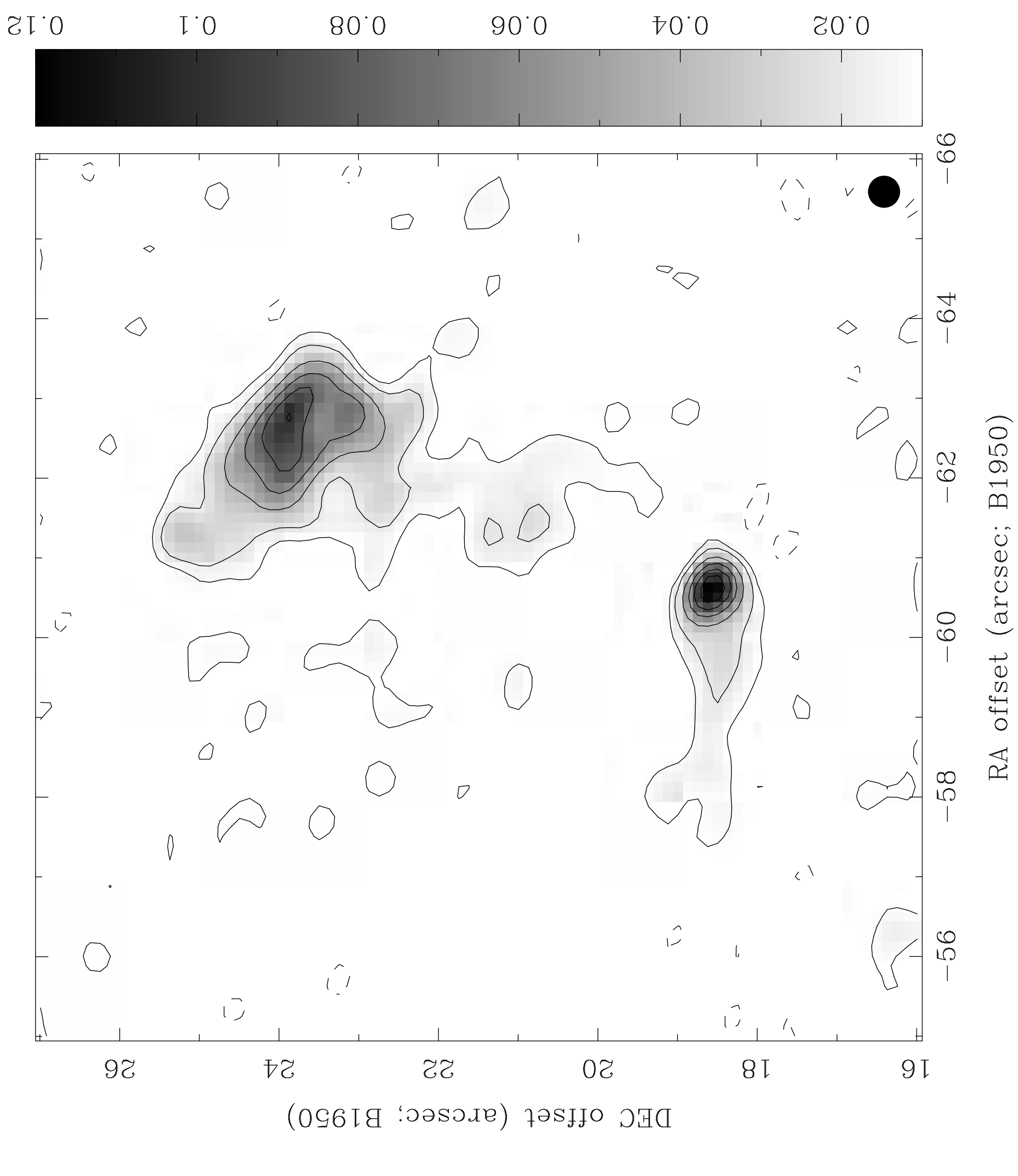

Fig. 6.— fig2 - South East hot spots D and E

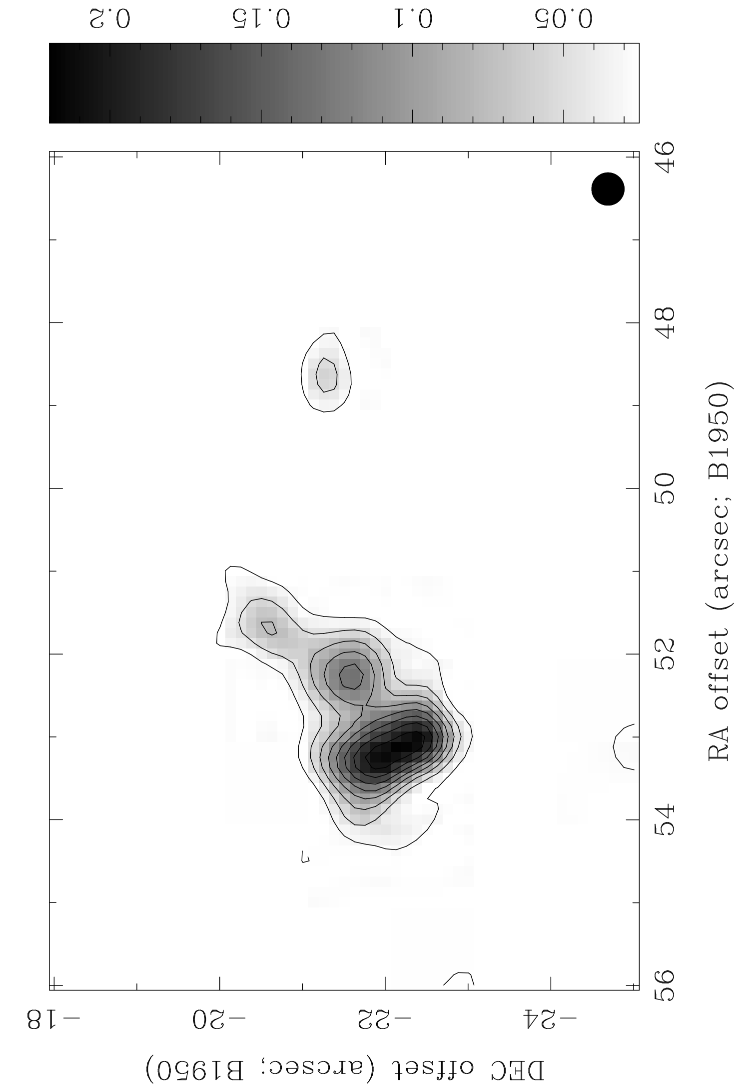

Fig. 7.— fig3 - North West hot spots A and B

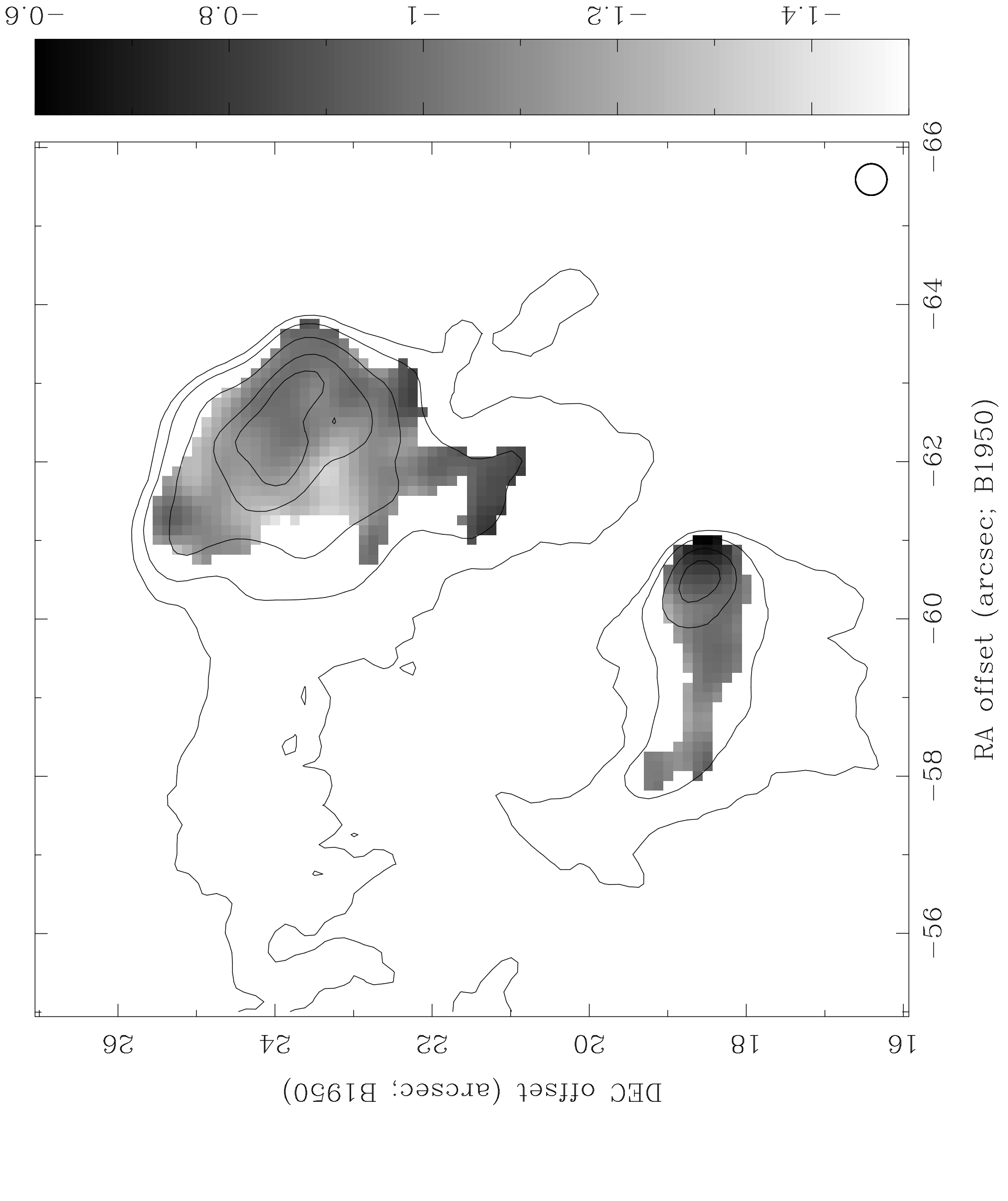

Fig. 8.— fig4 - South East hot spots D and E